ORIGINAL ARTICLE

Mixed-mode fracture toughness of high strength FRC: a realistic experimental approach

M. A. Hussien[1] · M. Moawad[1] · M. H. Seleem[1] · H. E. M. Sallam[1] · H. M. El-Emam[1]

Abstract

Unfortunately, fibrous composite materials' mixed-mode fracture toughness (K_{eff}) was measured using inappropriate through-thickness cracked (TTC) specimens. The problem with such specimens is the ignorance of the fibers in the pre-notch surfaces, i.e., no fiber bridging behind the crack tip. In the present paper, a real K_{eff} of fiber-reinforced concrete (FRC) was experimentally determined using matrix cracked (MC) specimens. Traditional (TTC) specimens were also adopted for comparison. The effect of fiber length (35 mm, 50 mm, and hybrid fibers, 50% from each length) and mode of mixity (M^e), $M^e = 0$, 1/4, and 1/2 were studied. Hooked end steel fibers of a volume fraction equal to 1% were used. All cracked beams with a crack-length-to-beam-depth ratio equal to 0.3 were tested under three-point bending in mode I and mixed-mode. The span/depth ratio was equal to two for all specimens. Since there is no equation to predict the K_{eff} of MC specimens and the inapplicability of Griffith's theory to predict the K_{eff} due to the difference in crack paths, new realistic procedures were suggested to overcome this dilemma. The results indicated that MC specimens recorded a lower crack initiation load than the peak load. In contrast, the crack initiation load coincides with the peak load in the case of TTC specimens. This reflected the role of steel fibers behind the crack tip in retarding the specimens to reach their ultimate capacity after crack initiation. K_{eff} increased with increasing M^e. Although long fibers recorded higher peak load and energy, their effect on K_{eff} of MC FRC specimens was marginal due to the minor effect of fiber length on the crack initiation loads. The MC specimen is a realistic approach for estimating the K_{eff} of FRC.

Keywords Mixed-mode fracture toughness · FRC · Mode of mixity · Matrix crack · Through-thickness crack

1 Introduction

Fiber-reinforced concrete (FRC) is a type of concrete that contains suitable discontinuous fibers added for a specific purpose. There is a wide variety of used fibers depending on material, shape, cross-section, and length. Fibers are

✉ H. E. M. Sallam
hem_sallam@zu.edu.eg; hem_sallam@yahoo.com

M. A. Hussien
mahmoudattia847@gmail.com

M. Moawad
mamoawad84@gmail.com

M. H. Seleem
mhseleem1963@gmail.com

H. M. El-Emam
elemamh@yahoo.com

[1] Materials Engineering Department, Faculty of Engineering, Zagazig University, Zagazig 44519, Egypt

commonly used in concrete to increase the toughness and avoid cracking due to shrinkage during the plastic and drying stages. Furthermore, permeability and water bleeding can be limited by using FRC. In some cases, larger steel or synthetic fibers can replace rebar or steel reinforcement [1]. FRC resistance to tensile cracking made it the best in the tension side of functionally graded concrete (FGC) beams with different patterns of FRC, normal weight concrete, and lightweight concrete [2]. Therefore, the cracking of FRC during fracture is an important part of its global behavior.

The cracks may exist in FRC as one of the three common fracture modes [3] (mode I, mode II, and mode III) or mixed mode. In response to this fact, many researchers paid a huge effort to characterize the fracture properties of FRC. Many models were developed based on the nonlinear elastic fracture mechanics to describe mode I crack propagation in concrete. Examples of these models are the fictitious crack model by Hilerborg [4], the two-parameter fracture model [5], the crack band model [6], and the size effect model by

Bazant [7]. The research of mode I in concrete was compiled in recommendations and specifications like the RILEM committee (TC-50 FMC) [8]. On the other hand, studying the mixed-mode fracture is more difficult due to many challenges, such as local deformation near the crack tip [9], monitoring the length of crack extension [10], the theoretical analysis, and determining the crack initiation criteria. Although the researchers paid a lot of effort into investigating the mixed-mode fracture of FRC, they still cannot compile a specification or a committee report like mode I.

Using through-thickness cracked (TTC) specimens, various experimental setups and specimens were used to study the different combinations of mixed-mode loading, especially in tests of mixed-mode (I/II). The three-point bending (3 PB) specimen is still considered the most common setup used in mixed-mode cases. Fayed et al. [11] studied the contribution of mode II on mixed-mode fracture toughness (K_{eff}) using steel FRC composite. Arikan et al. [12] studied the effect of volume fraction (V_f) of textile glass fiber reinforced particle-filled polymer composite beams and different crack-length to beam-depth ratios (a/d). Carpinteri et al. [13] studied the effect of the water-to-cement ratio on *the K_{eff}* of FRC. Zhang et al. [14] used steel FRC in a new type of composite material and investigated the mixed-mode properties. The major shortage in the 3 PB setup is that the mode mixity (M^e) does not exceed 40% unless, in the case of using a span to depth ratio (S/d) equals two [15]. Another type of testing setup is the asymmetric four-point bending (A4PB) specimen, which can cover all the mixity cases from pure mode I to pure mode II. Many researchers used the A4PB setup to obtain K_{eff} of concrete, but there is disagreement in the applied formula to determine the geometry correction factor of mode I. He and Hutchinson [16] suggested a shape geometry factor for mode I (F_I), which agreed with the results obtained by Murakami [17] using finite element analyses. There was a slight difference in the results of F_I obtained by Zimmermann et al. [18] and the previous results due to using different equations. Shahani and Tabatabaei [19] suggested another equation to calculate F_I, but the results differed significantly. Jorbat et al. [20] investigated the mixed mode by testing the straight-notched Brazilian disc specimens. Another test setup is the semi-circular bending specimen, which showed good results in asphalt research. Using the same test setup, it can cover all mixity cases from pure mode I to pure mode II using inclined crack [11]. Therefore, Razmi and Mirsayar [21] used the cracked semi-circular bending specimens to study the mixed-mode (I/II) fracture toughness of jute fiber-reinforced concrete at different V_f and M^e.

Li et al. [22, 23] stated that there are two kinds of fracture mechanics criteria: global and local approaches. They found that the crack tip deformation (CTD) approach is considered a local approach directly correlated to the cracking mechanism at the crack tip. CTD vector is the equivalence of crack tip opening displacement (CTOD) and crack tip sliding displacement (CTSD), which can treat the crack growth problem as an event related to the whole system. Because CTD cannot treat the stress ratio, Hammouda and Sallam [24] proposed the CTD parameter (CTDP) to eliminate the effect of the stress ratio. Hammouda and co-workers [25–28] used the CTDP to check the capability of the concept to correlate fatigue crack growth (FCG) rate for different crack lengths under constant and variable amplitude loadings. The CTDP concept showed a capability to predict a crack initiated from through-thickness notches in monolithic materials [29, 30]. Therefore, El-Emam et al. [31, 32] applied the CTDP concept to study the stationary and fatigue crack growth of mixed-mode TTC in metallic materials.

Providing a reliable and usable post-cracking tensile strength transforms the brittle failure mechanism of plain concrete into a ductile failure mode in FRC [33]. The post-cracking behavior of FRC ranges from strain-softening to strain-hardening, depending on volume fraction, distribution, and geometry of fibers [1]. This material property provides major advantages to FRC, making the research interest in FRC fracture ever-present. It is worth noting that the TTC specimen is applicable for monolithic materials, as mentioned above. At the same time, the TTC specimen is not applicable for fibrous composite materials due to the absence of fiber bridging between the surfaces of the pre-crack. Therefore, for long fiber-reinforced polymers (FRP) laminates, El-Sagheer et al. [34] performed a matrix crack (MC) in FRP laminate like a real crack pattern to overcome this drawback in the standard test method for the fracture toughness estimation of FRP laminates (ASTM E1922) [35]. Their main objective was to avoid the lack of intact fibers behind the crack tip and find its intrinsic fracture toughness (K_{IC}).

Recently, the MC specimen was used to find the intrinsic value of K_{IC} in FRC and FGC for mode I cracked specimens. Elakhras et al. [36] used MC specimens to study the size effect on fracture toughness for FRC and FGC. They compared their results with Hillerborg's concept. The maximum size of the non-damaged defect (d_{max}) concept was used to judge the reliability of the results. Their proposed method showed more reliable results. Using the equivalent relationships of the two-parameter fracture model, Elakhras et al. [37] predicted K_{IC} for both FRC and FGC depending on load/crack mouth open displacement (CMOD) curve results of MC specimens. The size effect law and boundary effect model showed good compatibility when applied on FRC and FGC beams using MC specimens [38]. Ali et al. [39] applied the MC concept on FRC specimens subjected to mode I, investigating different a/d (0.1, 0.3, and 0.5) and fiber lengths (35 mm, 50 mm, and hybrid of them). They found that the MC specimen was a proper approach to measure the realistic value of K_{IC} for FRC.

As aforementioned, the MC specimen approach could consider the contribution of fiber bridging during the mode I crack propagation in FRC [36–39]. Checking this potential in mixed-mode MC specimens is an interest leading to a generalized realistic experimental approach. Therefore, the main objective of this paper is to compare the K_{eff} of TTC FRC specimens using previous approaches based on linear elastic fracture mechanics (LEFM) with K_{eff} estimated from the proposed MC specimen approach. This investigation will be carried out on FRC beams subjected to different mode mixities (I/II) and fiber lengths.

2 Hypothesis

Certainly, TTC specimens cannot predict fracture toughness in fibrous composite materials. In other words, the fracture toughness test results obtained with these specimens do not reflect the real circumstances of the members/components made from such materials. Unfortunately, such previous work was not only a waste of time and effort but also led the scientific research compass in this field in the wrong direction for solving such problems. The first attempt in the right direction for predicting the fracture toughness of fibrous composite materials was made by Salam and colleagues [34, 36–39]. Sallam and co-workers [36, 39] successfully correlated the mode I fracture toughness of FRC using MC specimens, i.e., correlating a vectorial problem with a crack path independent of the initial crack length by scalar parameters such as Griffith's energy release rate.. The dilemma of the proposed work is that mixed-mode fracture toughness is a vectorial problem with a crack path dependent on either initial crack length or M^e, as shown in Fig. 1. Therefore, Griffith's energy release rate is inappropriate for measuring fracture toughness in such cases.

Recall some of the ideas that have succeeded in overcoming such challenges before to generate a new accurate idea for determining the mixed-mode fracture toughness of MC

specimens. In 1990, Sallam [40] measured the FCG rate in stiffened panels using specimens with different initial crack lengths. Due to the lack of closed-form solutions for calculating stress intensity factors (SIFs) in stiffened panels, this problem was resolved by applying the following technique using the master curve of FCG rate vs. SIF range for an unstiffened panel: (a) In the stiffened panel, a curve was drawn between FCG rate and crack length, (b) the master curve of FCG rate vs. SIF range of unstiffened panel was established, (c) and the SIF range in stiffened panel vs. the crack length was obtained by equating the FCG rate, as shown in Fig. 2. Moreover, El-Emam et al. [32] adopted this procedure to compare the numerical prediction of SIF in cracked steel plates strengthened with a composite patch with those measured experimentally by Wang et al. [41].

Such a technique can be adopted to get mode I SIF (K_I) and mode II SIF (K_{II}) separately and finally K_{eff} ($\sqrt{K_I^2 + K_{II}^2}$) of
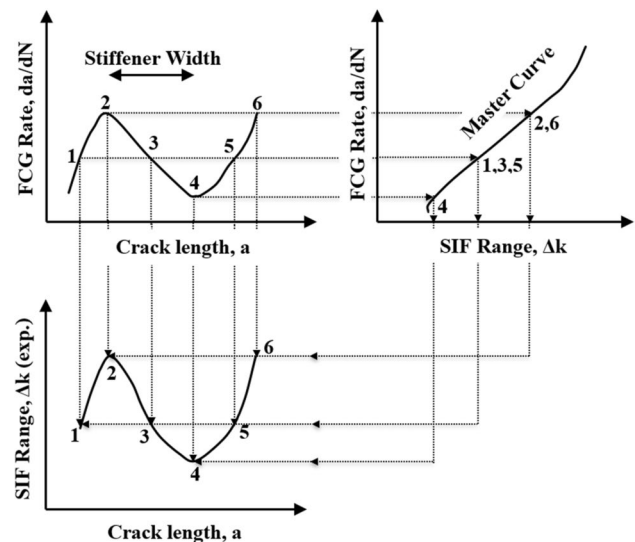
Fig. 2 Determination of SIF range in stiffened panels experimentally

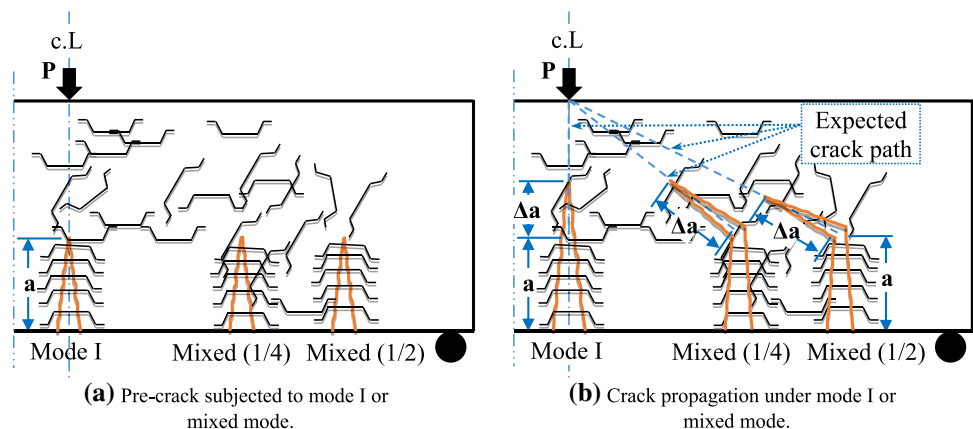**Fig. 1** Schematic diagram for different mode mixity

(a) Pre-crack subjected to mode I or mixed mode.

(b) Crack propagation under mode I or mixed mode.

Fig. 3 Schematic diagram for the proposed procedure to get the mixed-mode fracture toughness of matrix cracked specimens
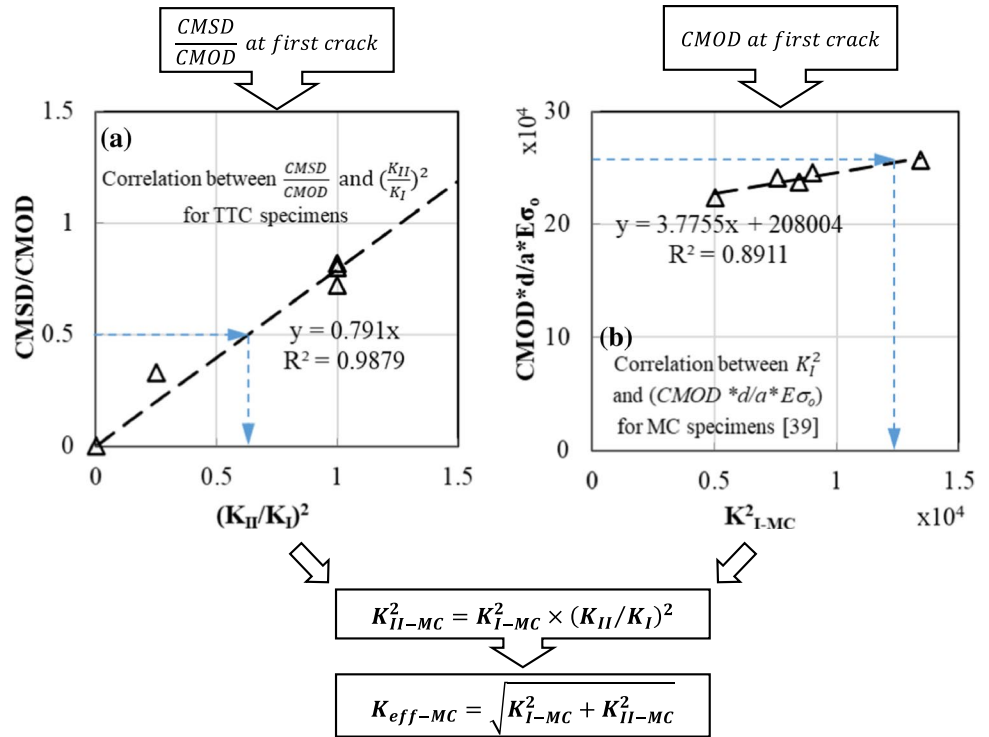
$\dfrac{CMSD}{CMOD}$ *at first crack*

CMOD at first crack

(a) Correlation between $\dfrac{CMSD}{CMOD}$ and $\left(\dfrac{K_{II}}{K_I}\right)^2$ for TTC specimens

$y = 0.791x$
$R^2 = 0.9879$

$y = 3.7755x + 208004$
$R^2 = 0.8911$

(b) Correlation between K_I^2 and $(CMOD * d/a * E\sigma_o)$ for MC specimens [39]

$$K_{II-MC}^2 = K_{I-MC}^2 \times (K_{II}/K_I)^2$$

$$K_{eff-MC} = \sqrt{K_{I-MC}^2 + K_{II-MC}^2}$$

Table 1 Geometry correction factors for mode I and mode II at $a/d = 0.3$, and $S/d = 2$ at different M^e

Geometry factors, according to Fett [15]	Mode mixity		
	Mode I	Mixed (1/4)	Mixed (1/2)
F_I	0.5655	0.32	0.17
F_{II}	0	0.13	0.17

MC specimens will be obtained as follows: (a) Firstly, a master curve of the ratio of CMOD to the crack mouth sliding displacement (CMSD), CMSD/CMOD, vs. $(K_{II}/K_I)^2$ for TTC specimens will be obtained, as shown in Fig. 3a. To get the master curve shown in Fig. 3a, the fracture toughness of TTC specimens was calculated at first crack initiation using the following relation suggested by Fett [15]:

$$K_I = \sigma_o F_I \sqrt{\pi a} \tag{1}$$

$$K_{II} = \sigma_o F_{II} \sqrt{\pi a} \tag{2}$$

Table 1 represents the values of the geometry correction factors F_I and F_{II} for $a/d = 0.3$ and $S/d = 2$. Where σ_o is the flexural stress at the first crack, and "a" is the crack length. The measured critical values of CMOD and CMSD for different M^e are listed in Table 2.

Once a relation between CMSD/CMOD vs. $(K_{II}/K_I)^2$ was established in Fig. 3.a, it is assumed that this relation is valid also for MC specimens. Then the relation between CMSD/CMOD vs. K_{II}/K_I for MC specimen was obtained, (b) recall the relation between CMOD and mode I SIF (K_I)^2 was obtained previously by the authors [39], as shown in Fig. 3b. Knowing the relation between CMSD/CMOD vs. $(K_{II}/K_I)^2$ for the MC specimen and the relation between the CMOD vs. $(K_I)^2$ for the MC specimen can easily get K_{II} for the MC specimen. Finally, K_{eff} was obtained, as shown in Fig. 3.

Table 2 Critical values of CMOD and CMSD in mm

Fiber length $(L_f)^a$	$M^e = 0.25$			$M^e = 0.5$		
	CMOD	CMSD	CMSD/CMOD	CMOD	CMSD	CMSD/CMOD
SF				0.2415	0.180	0.745
LF	0.248	0.078	0.314	0.2420	0.210	0.867
HF				0.2422	0.225	0.930

[a]Short fiber (SF), $L_f = 35$ mm, long fiber (LF) $L_f = 50$ mm, and HF: a hybrid between 35 and 50 mm with equal ratios of 50%

3 Experimental work

3.1 Experimental program

An experimental program consisting of seventeen groups of beams was used to investigate the behavior of K_{eff} of MC and TTC FRC specimens. Three identical specimens were used to represent each case study. The dimensions of all specimens were 150 mm in depth (d), 200 mm in width (B), and 500 mm in length (L). All beams were tested under 3 PB over a span (S) of 400 mm, and S/d equals 2. Eight pre-cracked beam specimens with different crack offsets (C) from the beam center ($C = 0.54d$ and $0.725d$) were used to study the effect of M^e ($M^e = 1/4$ and $1/2$) on K_{eff}. The effect of three steel fiber lengths (L_f) with a constant V_f equal to 1% was studied. The fiber lengths were 50 mm (LF), 35 mm (SF), and hybrid fibers of 50%

LF and 50% SF (HF). Furthermore, three uncracked (UC) specimens and six pre-centered cracked specimens were used to estimate K_{IC}. The cracked specimens were divided into two equal groups with two different crack surface patterns (TTC and MC) with a/d equal to 0.3. The details of the studied beams are shown in Fig. 4, and the studied parameters are listed in Table 3.

3.2 Materials characterization

The constituent materials are grade 52.5 N-type I ordinary Portland cement, natural siliceous sand as fine aggregate, and dolomite with a maximum aggregate size (NMAS) of 12.5 mm as coarse aggregate. Properties of the used fine and coarse aggregates are found in Table 4. Silica fume by 10% as partial replacement of cement by weight was used to produce high strength FRC. The properties of the used silica fume are given in Table 5. Master-Glenium
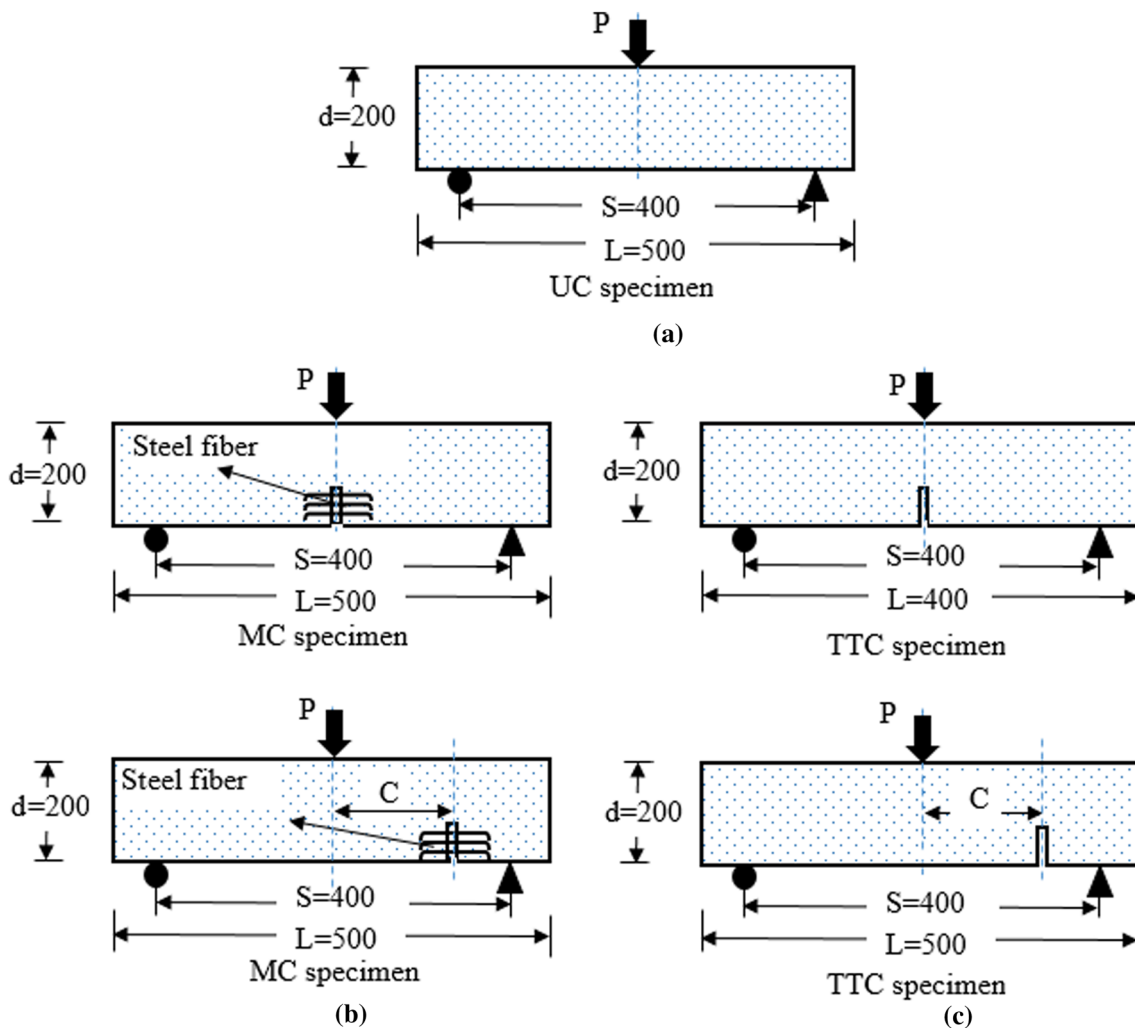

Fig. 4 Details of tested beams **a** UC, **b** MC, and **c** TTC beams; all dimensions are in mm

Table 3 Details of the tested beams

Specimen ID	Mode of mixity(M^e)	Crack surface	Steel fibers length, L_f (mm)
UC-SF	–	UC	35
UC-LF	–	UC	50
UC-HF	–	UC	Hybrid
MC-SF (0)	Mode I	MC	35
MC-LF (0)	Mode I	MC	50
MC-HF (0)	Mode I	MC	Hybrid
TTC-SF (0)	Mode I	TTC	35
TTC-LF (0)	Mode I	TTC	50
TTC-HF (0)	Mode I	TTC	Hybrid
MC-SF (1/2)	Mixed (1/2)	MC	35
MC-LF (1/2)	Mixed (1/2)	MC	50
MC-HF (1/2)	Mixed (1/2)	MC	Hybrid
MC-LF (1/4)	Mixed (1/4)	MC	50
TTC-SF (1/2)	Mixed (1/2)	TTC	35
TTC-LF (1/2)	Mixed (1/2)	TTC	50
TTC-HF (1/2)	Mixed (1/2)	TTC	Hybrid
TTC-LF (1/4)	Mixed (1/4)	TTC	50

Identification of specimens starts with crack surface patterns (*UC* uncracked, *MC* matrix crack, *TTC* through-thickness crack), followed by fiber length (short fiber (SF), $L_f = 35$ mm, long fiber (LF) $L_f = 50$ mm, and HF: a hybrid between 35 and 50 mm with equal ratios of 50%). The mode of mixity is added at the end in two brackets (0: $C = 0$, 1/4: $C = 0.54\ d$, and 1/2: $C = 0.725\ d$)

Table 4 Properties of fine and coarse aggregates

Property	Sand	Dolomite
Specific gravity, G_s	2.57	2.67
γ_{loose}, kg/m³	1610	1500
$\gamma_{compacted}$, kg/m³	1680	1560
Percentage voids	37.2%	41.57%
Fineness modulus	2.4	–
Percentage absorption	–	0.6%
Crushing value	–	21%

Table 5 Properties of silica fume

Color	Light gray
Specific gravity	2.20
Bulk density	350 kg/m³
Specific surface area	16.7 m²/gm

RMC 315 (from BASF COMPANY) was used as a super-plasticizer. Hooked-end steel fibers with a tensile strength of 1100 MPa, an ultimate elongation of 2%, and specific gravity of 7.85 were used to produce FRC. The fibers are characterized by 35 mm and 50 mm lengths, with aspect ratios of 43.75 and 50, respectively.

The ACI 544.3R-08 [42] procedures for designing FRC mixes were followed to estimate the proportions of the constituent materials of the FRC mix. The quantities of materials required to produce one cubic meter from the FRC mix are given in Table 6. The mixing procedures, casting, and curing were performed following the instructions of the ACI committee of the FRC [42]. According to BS EN 12390-3 [43], cubes of dimensions $150 \times 150 \times 150$ mm were used to measure the compressive strength of concrete. Cylinders of 150 mm diameter and 300 mm height were used to measure the indirect tensile strength according to BS EN 12390-6 [44]. Double L shape specimens [45] were used to calculate the shear strength. The previous specimen was used for reinforced concrete to calculate the shear strength [46]. All specimens were cured in fresh water and tested after 56 days. The mechanical properties of the hardened three mixes of FRC are presented in Table 7. The mean values and their coefficient of variance are reported in the table.

3.3 Creation of MC and TTC

The TTC was made using a foam plate having 2 mm thickness, 150 mm width, and 60 mm height. The plate was fixed at different distances from the beam center depending on M^e using a groove at the desired position on each longitudinal side of the steel mold. The same type of foam was used for the MC with the same dimensions. The steel fibers were located in their positions, as shown in Fig. 5. It was assumed that the fibers were distributed uniformly through the plate surface. The same procedure for estimating the number of fibers crossing the foam plate [36] was followed. Therefore, one-third of the volume fraction of steel fibers bridged the preformed crack. The number of fibers crossing the crack was assumed constant irrespective of the fiber length to monitor the effect of fiber lengths on K_{eff}.

3.4 Instrumentation and test setup

A servo-hydraulic universal testing machine of 1000 kN maximum capacity was used for testing all beams at the

Table 6 Constituents materials in kg required to produce 1 m³ from FRC

Cement	Silica fume	Sand	Dolomite	Water	Superplasticizer	Steel fibers
495	55	740	915	171	11	78.5

specified age. The beams were supported over a span of 400 mm and tested under a 3 PB configuration. A load cell of 300 kN maximum capacity was used to measure the load. Three linear variable displacement transducers (LVDT) of 0.001 mm sensitivity were used to measure the mid-span deflection, CMOD, and CMSD. The test setup

Table 7 Mechanical properties of the used FRC mixtures

Property	Fiber length, mm[a]		
	35	50	Hybrid
Compressive strength, MPa	68.64 (0.019)[a]	64.70 (0.013)[a]	65.30 (0.016)[a]
Tensile strength, MPa	6.50 (0.040)	7.80 (0.061)	7.30 (0.064)
Flexural strength, MPa	14.00 (0.049)	13.00 (0.046)	13.00 (0.040)
Shear strength, MPa	6.96 (0.100)	8.19 (0.075)	5.10 (0.088)

[a]Values in the parentheses indicate the coefficient of variance (dimensionless)
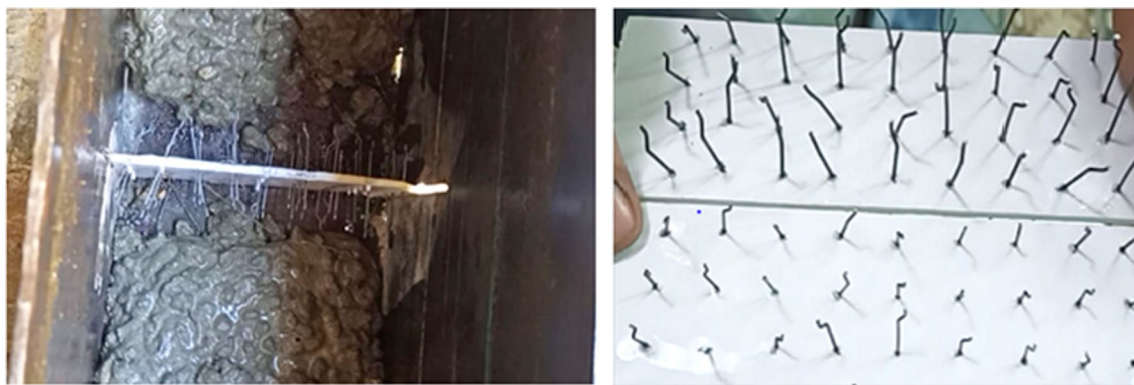
Fig. 5 Matrix crack preparation
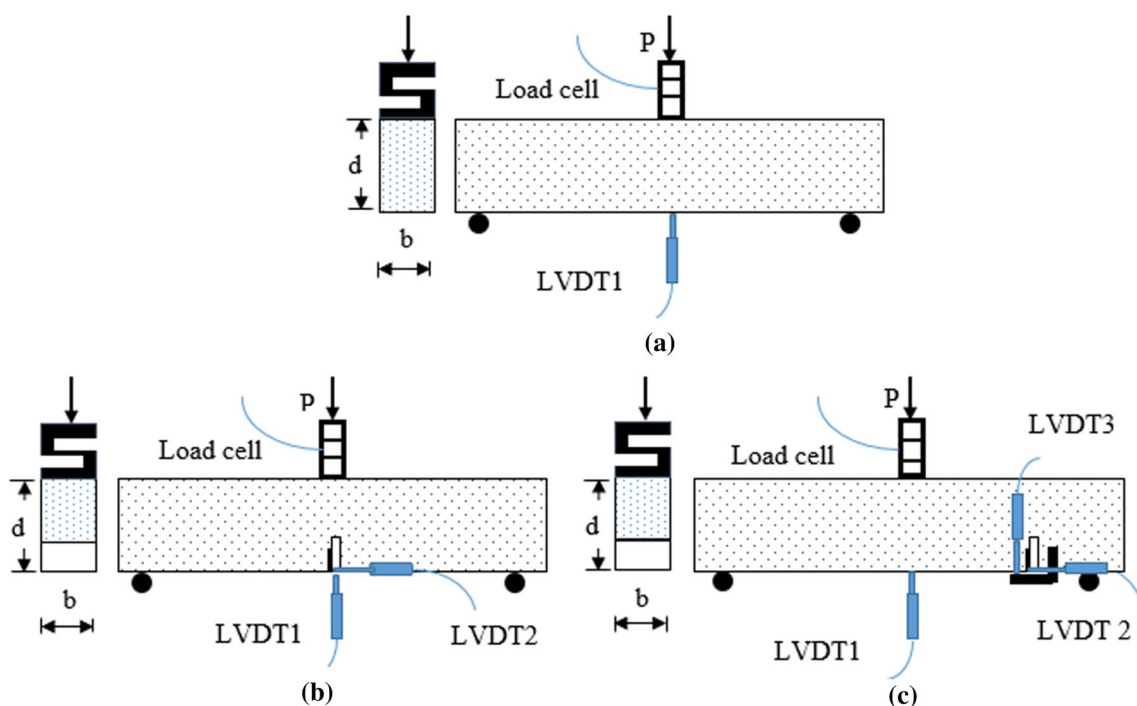
Fig. 6 Instrumentations and test setup for **a** UC, **b** mode I, and **c** mixed-mode beams

and instrumentations for uncracked and cracked specimens are shown in Fig. 6.

4 Results and discussion

Samples from the load–deflection (P–δ) curves representing UN, MC, and TTC specimens are shown in Fig. 7. Each figure shows the P–δ curves of the three specimens tested for each case study. The ascending and descending portions of P–δ curves for each set were fitted using the multi-linear curve suggested by Mubarki et al. [47], as indicated by the solid lines in Fig. 7. The points of the fitted curve represent the destinations of the slope changes. The fitted curve quality was tested statistically using the regression factor (R^2). The values of R^2 show a high quality of the fitting, as shown in Fig. 7. Therefore, the fitted curves were used to analyze and discuss the test results.

4.1 MC versus TTC beams

The effect of the crack surface pattern (MC or TTC) on the P–δ, load-CMOD (P-CMOD), and load-CMSD (P-CMSD) behavior for different steel fiber lengths under modes I and M^e equal 1/2 is shown in Figs. 8 and 9, respectively. However, Fig. 10 shows this effect for a fiber length equal to 50 mm under M^e equals 1/4. Regarding the P–δ curves, the small degradation in MC specimens reflects the role of fibers bridging the crack in maintaining the most capacity of the UC specimens. MC specimens recorded higher peak loads compared to TTC specimens. The trends of P-CMOD and P-CMSD are similar to P–δ curves for both MC and TTC specimens, as shown in Figs. 8, 9 and 10.

The figures indicated that in MC specimens where fibers bridge the crack surface, there is a drop in the slope of the P–δ curve at a point corresponding to the crack initiation before the peak load. This means that the crack initiation load is lower than the peak load in the MC specimens. In the case of TTC specimens, the results indicated that the crack initiation occurred at the peak load. This reflects the role of steel fibers behind the crack tip in retarding the specimens

to reach their ultimate capacity after crack initiation. Also, it is observed that the drop in the applied load after the peak occurs gradually in the case of MC, while it occurs sharply in the case of TTC. This observation is more obvious for specimens subjected to Mode I, as shown in Fig. 8. The figures also show higher areas under the P–δ curves for MC specimens than TTC specimens, especially in the descending portion of the curves.

The peak loads for the MC and TTC specimens for mode I and mixed-mode of different M^e and fiber lengths are given in Table 8. The ratios of peak loads due to the MC pattern compared to the TTC pattern are presented in the table. As mentioned above, higher peak loads were observed in the case of MC specimens compared to TTC specimens, irrespective of the fiber length, type of mode, or M^e. For mode I, the peak load ratios between MC and TTC were 325.58%, 353.85%, and 344.44% for SF, hybrid, and LF, respectively. However, these ratios were 165.63%, 153.95%, and 160.53% for SF, hybrid, and LF, respectively, for specimens subjected to mixed mode (M^e = 1/2). For the mixed mode of M^e equals 1/4 and L_f = 50 mm, this ratio was 247.83%.

The total energy (G_t) for all MC and TTC specimens was calculated up to deflection equals seven mm (0.035d) by estimating the area under the fitted P–δ curve up to this deflection value. These results are presented in Table 9. The ratios of G_t for MC specimens to TTC specimens are also presented in the table. Higher ratios of G_t were recorded in the case of MC specimens compared to TTC specimens irrespective of the fiber length, type of mode, or M^e. For mode I, G_t ratios between MC and TTC were 292.2%, 460.5%, and 250.6% for SF, hybrid, and LF, respectively. However, these ratios were 188.6%, 220.5%, and 147% for SF, hybrid, and LF, respectively, for specimens subjected to mixed mode (M^e = 1/2). For the mixed mode of M^e equals 1/4 and LF, the percentage difference in the toughness was 217%. The difference in G_t of MC specimens as compared to TTC specimens reflects the contribution of the reinforcement area by steel fibers bridging the crack surface behind the crack tip in MC specimens in enhancing the capability of the cracked specimens to carry additional load after the maximum and before failure compared to TTC specimens.

Fig. 7 Samples of experimental and fitted P–δ curves for UC, MC, and TTC beams
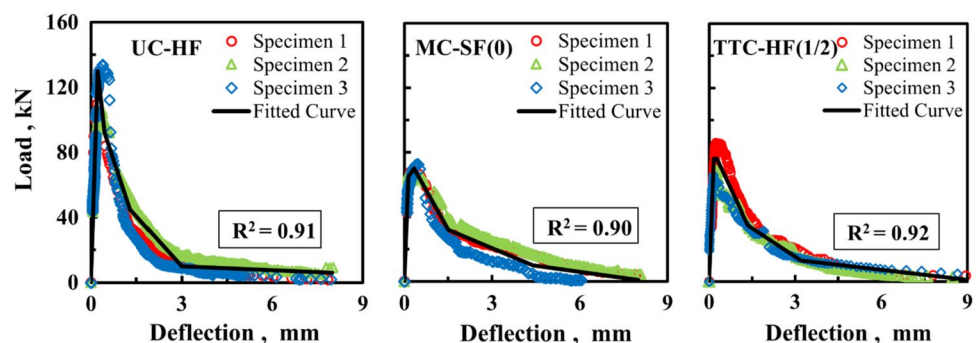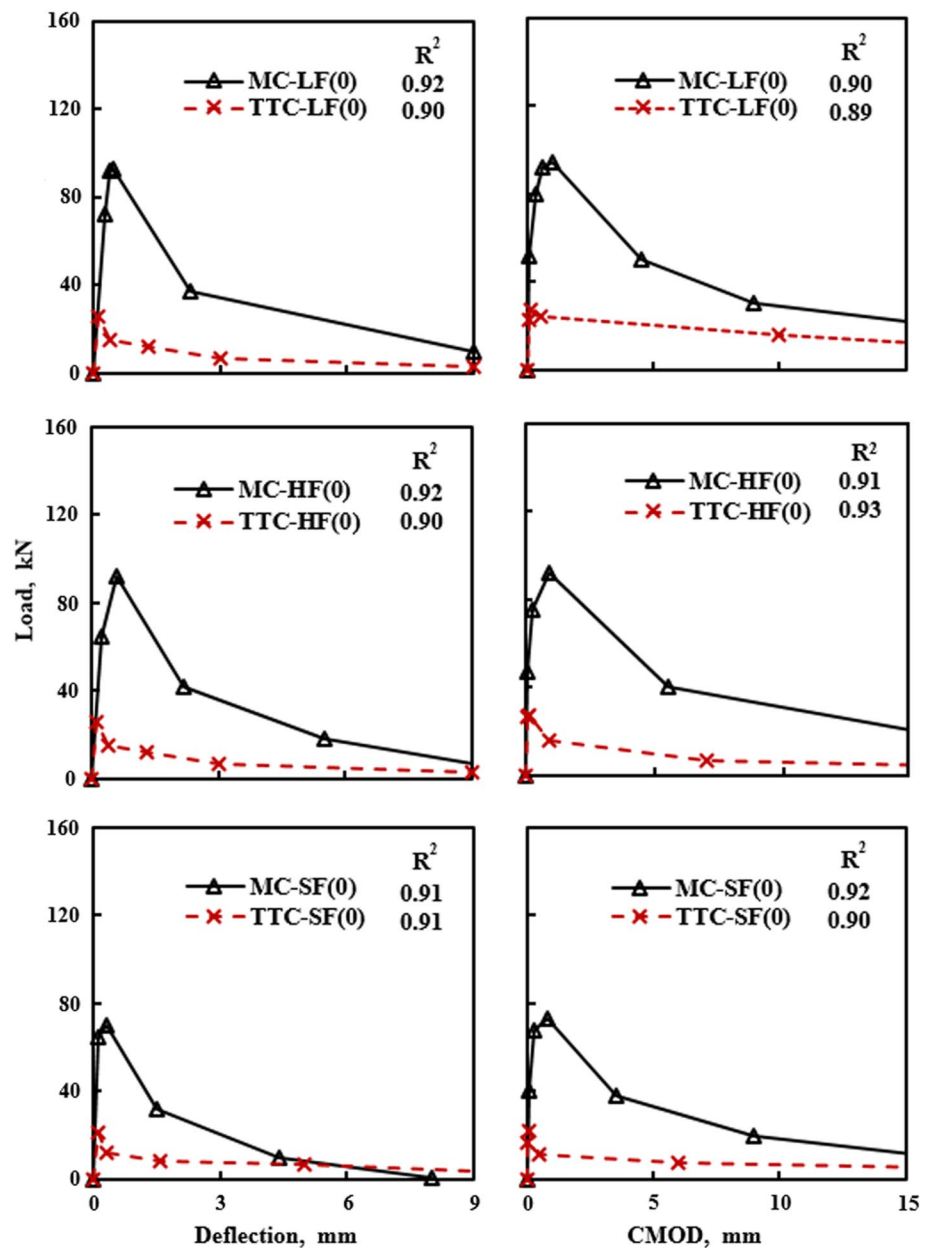
Fig. 8 Load–deflection and P-CMOD behaviors for different fiber lengths under mode I for MC and TTC beams

The analysis mentioned above indicates that using a TTC pattern cannot be correctly used to estimate the fracture toughness of FRC beam specimens. It produces severe degradation in stiffness, peak loads, and total energy up to fracture compared to the real degradation of the cracked elements. Thus, the real fracture toughness must be estimated using the MC specimens where the crack passes through the matrix while fibers are still bridging the crack.

It is worth mentioning that the effect of fiber length on the results of TTC beams agrees with the results obtained by Ali et al. [39] and Chang and Chai [48] for TTC FRC specimens subjected to mode I. Also, it agrees with the results of different mixity ratios studied by Qing et al. [49]. They studied steel fiber and aligned it with different V_f at different

C (from 0 to 0.75). They found that the peak load increased by 220% at $a/d = 0.3$ and C = 0.75 in the case of steel fiber. The present study showed close ratios at C = 0.725; the peak load increased by 197% and 192%, and 181% using SF, HF, and LF. Nunes and Reis [50] found that the K_{eff} increased by about 25.7% in the case of C = 0.6. According to the current study, K_{eff} increased by about 35.8%, 35.5%, and 32.3% using SF, HF, and LF, respectively, at C = 0.725. Fayed et al. [11] studied the effect of different a/d (0.2, 0.3, 0.4, and 0.5) and different values of C (0, 0.25, 0.5, 0.75) using steel fiber at $S/d = 4$. Like the present study, they found that increasing the crack offset increased the M^e increasing K_{eff} up to C = 0.5 compared with K_{IC}. After this value of C, they found that K_{eff} decreased, which supports studying the maximum value of

Fig. 9 Effect of crack pattern on mixed-mode, $M^e = (1/2)$ for different fiber lengths
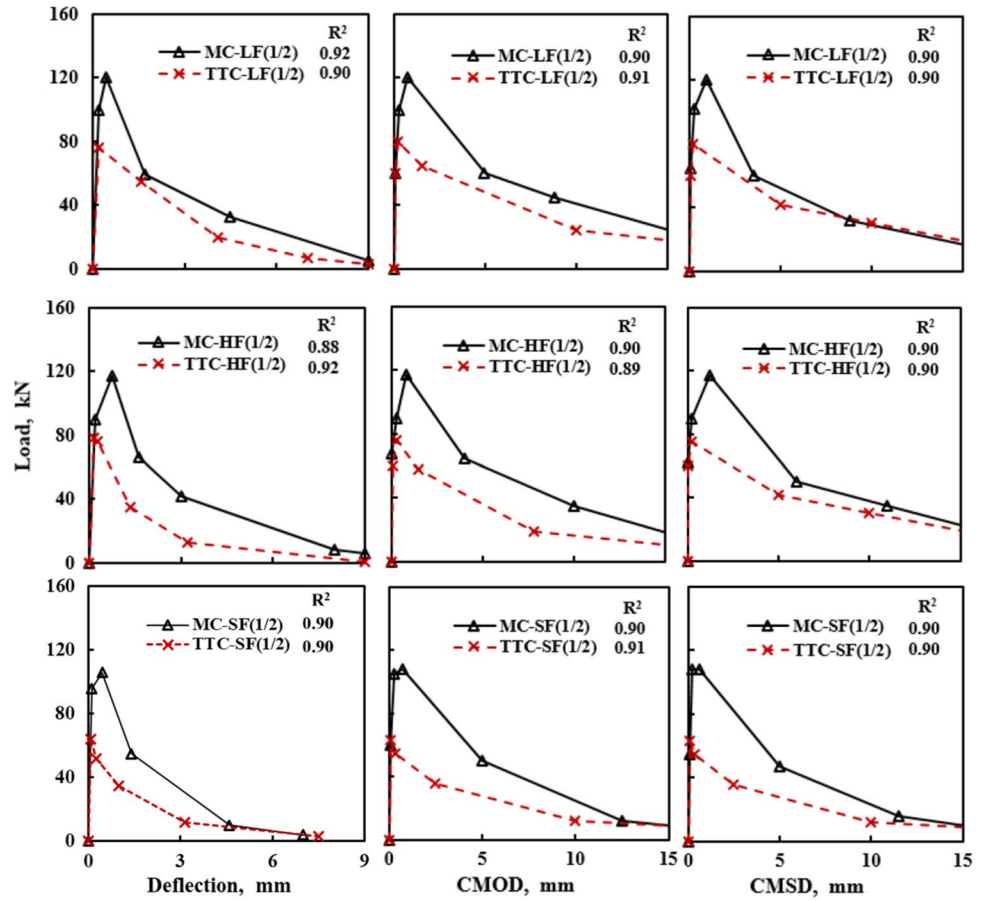

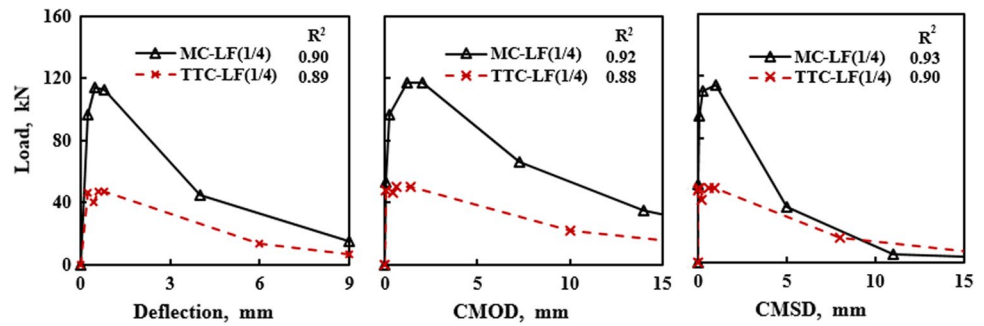**Fig. 10** Effect of crack pattern on P–δ, P-CMOD, and P-CMSD behaviors for LF under $M^e = 1/4$

Table 8 Peak loads for MC and TTC investigated beams

MC		TTC		(P_{MC}/P_{TTC}) *100
Beam code	P_{MC}, kN	Beam code	P_{TTC}, kN	
MC-SF (0)	70 (0.047)[a]	TTC-SF (0)	21.5 (0.107)[a]	325.58
MC-HF (0)	92 (0.041)	TTC-HF (0)	26 (0.023)	353.85
MC-LF (0)	93 (0.032)	TTC-LF (0)	27 (0.022)	344.44
MC-SF (1/2)	106 (0.071)	TTC-SF (1/2)	64 (0.051)	165.63
MC-HF (1/2)	117 (0.025)	TTC-HF (1/2)	76 (0.074)	153.95
MC-LF (1/2)	122 (0.021)	TTC-LF (1/2)	76 (0.090)	160.53
MC-LF (1/4)	114 (0.026)	TTC-LF (1/4)	46 (0.130)	247.83

[a]Values in the parentheses indicate the coefficient of variance (dimensionless)

Table 9 Total energy of MC and TTC investigated specimens

MC		TTC		$(G_{t\text{-MC}}/G_{t\text{-TTC}})$ *100
Beam code	G_{t}-MC, kN mm	Beam code	G_{t}-TTC, kN mm	
MC-SF (0)	155.5	TTC-SF (0)	53.2	292.2
MC-HF (0)	264.6	TTC-HF (0)	57.45	460.5
MC-LF (0)	303.6	TTC-LF (0)	121.17	250.6
MC-SF (1/2)	238.45	TTC-SF (1/2)	126.4	188.6
MC-HF (1/2)	332.2	TTC-HF (1/2)	150.6	220.5
MC-LF (1/2)	341.5	TTC-LF (1/2)	231.9	147.3
MC-LF (1/4)	433	TTC-LF (1/4)	199.5	217

Table 10 Real K_{eff} for MC FRC specimens

Beam code	K_{eff}, MPa mm$^{0.5}$
MC-SF (0)	104
MC-HF (0)	104
MC-LF (0)	102
MC-SF (1/2)	124
MC-HF (1/2)	121.8
MC-LF (1/2)	121
MC-LF (1/4)	114

specimens, and the results are given in Table 10. To check the reliability of the present method for estimating the fracture toughness of FRC, the concept of the non-damage defect zone (d_{max}) [24] was used. In this concept, d_{max} is equal to $\frac{1}{\pi}\left(\frac{K_I}{1.12\times\sigma_0}\right)^2$. Where K equals K_{IC} in the case of mode I [51], K_{IIC} in mode II [52], and K_{eff} in the case of mixed mode. The d_{max}/NMAS were calculated, and the results are given in Table 11. The ratios of d_{max}/NMAS in the current study ranged between 1 and 2 in MC specimens, near the ratios found by Elakhras et al. [36–38] for mode I, which were greater than unity.

Furthermore, the current d_{max}/NMAS ratios are near the results obtained by Ali et al. [39] for MC specimens of $S/d=4$ and subjected to mode I at different a/d and fiber lengths. A comparison between the values of K_{Ic} measured at $a/d=0.3$ for different specimen sizes, i.e., $S/d=2$ (present study) and $S/d=4$ [39] are listed in Table 12. The K_{Ic} values decreased by increasing the specimen size, which is compatible with the size effect law. In the case of short fiber, the K_{Ic} decreased by 7%, while K_{Ic} decreased by 11% for long fiber. It can be concluded that this decrement is dependent on the fiber length.

Table 11 The ratios of d_{max}/NMAZ for MC FRC specimens

Beam code	d_{max}/NMAZ
MC-SF (0)	1.13
MC-HF (0)	1.3
MC-LF (0)	1.25
MC-SF (1/2)	1.6
MC-HF (1/2)	1.78
MC-LF (1/2)	1.75
MC-LF (1/4)	1.56

Likewise, the current trend of K_{eff} in MC specimens is compatible with the trend of K_{IC} in mode I, which was found by Ali et al. [39] experimentally and El-Sagheer et al. [34] numerically. Like the present study, they found that the MC specimens with short fiber produced higher fracture toughness. This finding reflects the good capability of the MC approach to get an intrinsic value of K_{eff}, like its capability to get K_{IC}.

$M^e=0.5$ in the present study. They found, in some cases, the failure did not start from the notch, while it took place from the bottom of the specimen beneath the loading point. Similar findings were found when using different setups, materials, and mode mixity [18–20].

Therefore, the MC approach needs to be simplified in a robust equation at different sizes, a/d, M^e, and test setups.

4.2 Real fracture toughness of MC FRC

The procedures mentioned before in Sect. 2 were used to calculate the intrinsic values of K_{IC} and K_{eff} for MC

Table 12 Effect of specimen size on Real K_{IC} for MC FRC specimens at $a/d=0.3$

Beam code	K_{IC}, MPa.mm$^{0.5}$		Ratio, Short($S/d=2$)/long($S/d=4$)
	Present work	Ali et al. [39]	
MC-SF (0)	104	97	1.07
MC-HF (0)	104	95	1.09
MC-LF (0)	102	92	1.11

This simplification means too many extended experimental campaigns to get the required functions of geometry correction factors, which means more cost, effort, and time. The finite element simulation is a very good candidate for obtaining the geometry correction factors of MC specimens, which avoids exaggerated experimental work. On the other hand, Carpinteri [53] and Balush et al. [54] paid a lot of effort to obtain the geometry correction factor of the cracked reinforced concrete beam, i.e., a single fiber (one steel bar). Accordingly, the simulation of fiber arrays in the case of FRC requires multiple and painstaking efforts. To get accurate and useful results, this needs a well-planned study in the future. In this future study, it will be significant to execute an extensive numerical work plan to obtain the geometry correction factor of the MC specimen considering the effect S/d, a/d, M^e, and the properties of fibers, i.e., types, geometries, end condition, volume fractions, orientations, arrangement, and their mechanical properties.

4.2.1 Effect of fiber length

The effects of steel fiber length (SF, HF, and LF) on the P–δ behavior of UC, MC under mode I, and MC under mixed-mode FRC beams are shown in Fig. 11. The SF, HF, and LF show similar P–δ behavior in the three cases of UC and MC specimens under mode I or mixed mode. The UC specimens reinforced by SF show higher initiation and peak loads than those reinforced by LF. This may be due to the increased number of fibers for the same V_f of 1% as the fiber length decreased from 50 to 35 mm. The SF and LF show approximately identical descending portion behavior. On the other hand, the status is different in the case of UC specimens with HF, where the fibers are randomly distributed according to mixing and casting conditions. It was observed that the UC specimens with HF show lower descending parts compatible with the logic expected trend. This is due to the small number of fibers bridging the damaged sections of these specimens, as inspected visually.

As mentioned above, similar behavior was observed for cracked specimens, either subjected to mode I or mixed mode. The SF shows the lower descending part of the curve,

while LF and HF are nearly identical. The LF recorded a higher peak load than the SF or HF, see Table 8. For MC specimens subjected to mode I, increasing fiber length from 35 to 50 mm increased the peak load by about 32.85% while increasing by about 31.4% using HF. A similar trend was observed in the case of mixed mode, where the peak load increased by about 15.1% as the fiber length increased from 35 to 50 mm. On the other hand, utilization of HF increased the peak load by about 10.4% compared to SF. These results agree with the results obtained by Ali et al. [39] and Chang and Chai [48] for TTC FRC specimens subjected to mode I. They found that LF had a higher peak load and higher descending behavior than HF and SF. Although the difference in initial cracking load was not significant for mode I, the difference increased in mixed mode.

The effect of fiber length on G_t is similar to that of the peak load, see Table 9. For MC FRC specimens under mode I, increasing fiber length from 35 to 50 mm increased G_t by about 95.2%, while this increase was about 70% using HF. A similar trend was observed in the case of mixed-mode MC FRC beams, where G_t increased by about 43.2% as the fiber length increased from 35 to 50 mm. On the other hand, utilization of HF increased G_t by about 39% compared to SF (Fig. 12).
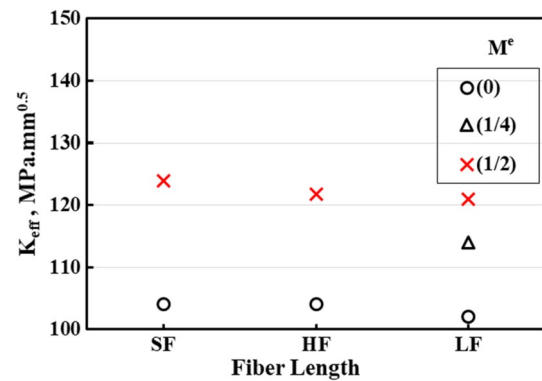
Fig. 12 The effect of fiber length on K_{eff} of MC specimens for different M^e

Fig. 11 Effect of fiber length on the P–δ behavior of MC specimens
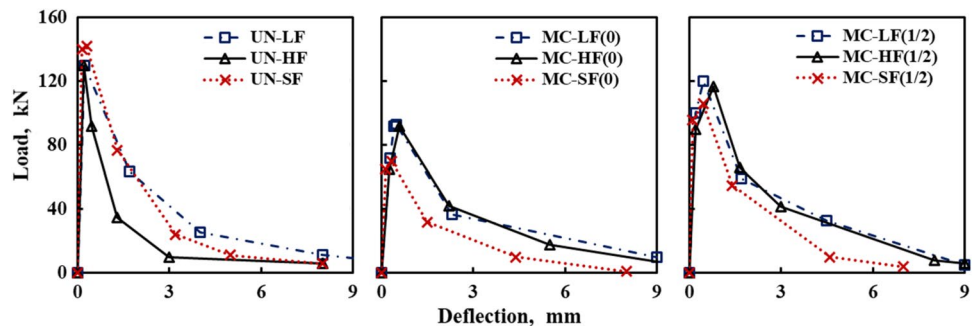
Fig. 13 Effect of M^e on the P–δ behavior of MC for different fiber lengths
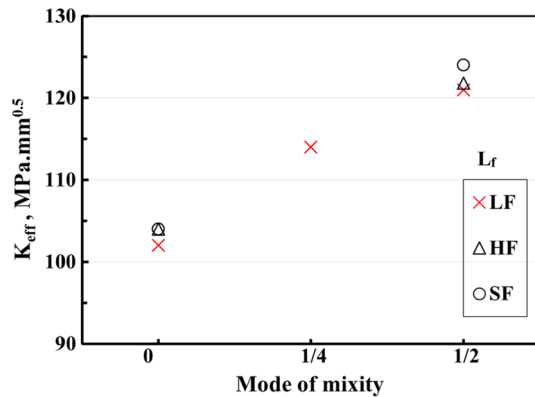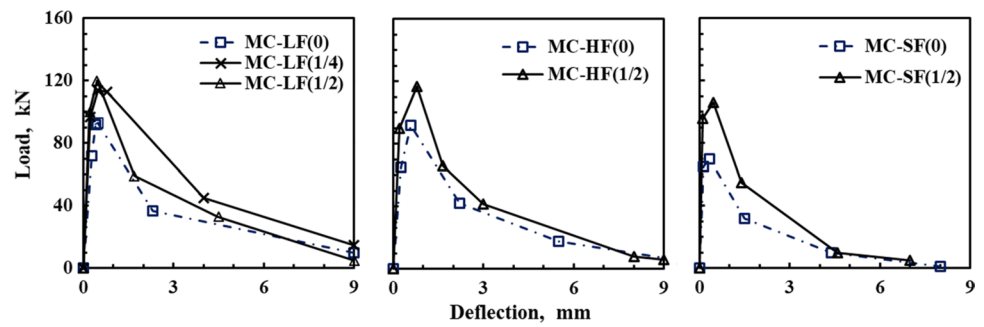

Fig. 14 Effect of mode of mixity on K_{eff} for different fiber lengths

The effect of fiber length on mode I and mixed-mode fracture toughness of MC FRC is given in Table 10 and illustrated in Fig. 13. For mode I, the effect of fiber length on K_{IC} is marginal. The SF and HF recoded the same K_{IC}, while the LF recorded a value lower by 2. This is because the number of fibers from each length bridging the crack is the same. Therefore, all lengths create approximately the same closing effect in the initial stages of loading up to the first crack initiation. The situation does not differ so much in the case of mixed mode. The SF recorded the higher K_{eff}, and the LF recorded the lower K_{eff}.

4.2.2 Effect of mixity mode

The effect of M^e on the P–δ behavior of MC FRC for SF, HF, and LF is shown in Fig. 13. The peak load generally increased when the fracture mode changed from mode I to mixed mode or increased M^e. The peak load increased by about 51.4%, 27.2%, and 31.2% for SF, HF, and LF when changing the fracture mode from mode I to mixed mode of M^e equals 1/2. On the other hand, increasing M^e from 1/4 to 1/2 increased the peak load by 7%. In the case of G_t, the trend is similar to that of the peak load, i.e., increasing M^e increased G_t irrespective of the fiber length. Increasing M^e from zero (mode I) to 1/2 (mixed-mode) increased G_t by 53.3%, 25.5%, and 12.5% for SF, HF, and LF. On the

other hand, G_t increased by about 12.5% as M^e increased from 1/4 to 1/2.

Generally, K_{eff} increased with increasing M^e, irrespective of the fiber length, as shown in Fig. 14. Increasing M^e from zero (mode I) to 1/2 (mixed-mode) increased K_{eff} by 19.2%, 17.1%, and 18.6% for SF, HF, and LF, respectively. On the other hand, increasing M^e from 1/4 to 1/2 increased K_{eff} by about 6.1%. These results agree with those results obtained by Qing et al. [49] and Nunes and Reis [50] using 3 PB. They found that when the notch location tended to the extreme of the beam span, the energy release rate and stress intensity factor for mixed-mode (I/II) loading values were larger than those of mode I. The results were similar when using different setups, materials, and mode mixity [18–20].

4.3 Fracture surface analysis

The crack trajectories for different M^e and fiber lengths were traced. The traces were categorized for each beam from the front and the back elevation, as shown in Fig. 15. The scattering in crack trajectories is not large. This may be due to the crack propagating through the coarse aggregate (transgranular crack growth), as shown in Fig. 16. The crack generates from the pre-crack for most specimens unless, in some specimens subjected to the mode of mixity equals 1/2, the crack generates from the bottom of the specimen beneath the loading point. These observations increased the reliability of the collected data from this study to investigate the effect of the mixity mode on the fracture toughness of FRC.

As a global overview of the current results, Figs. 15 and 16 represent the crack trajectories. It is noticed that the crack initiation angles are difficult to be measured due to the tortuosity in crack paths. The tortuosity in the crack may be due to the existence of steel fiber density that arrested the crack and forced it to deviate from the original initiation angle. The effect of steel fibers must be considered in the analysis to predict the actual crack path. Table 13 presents the mean number of steel fibers in the crack path area. The theoretical number was calculated according to Naaman's assumption [1] using the following equation:
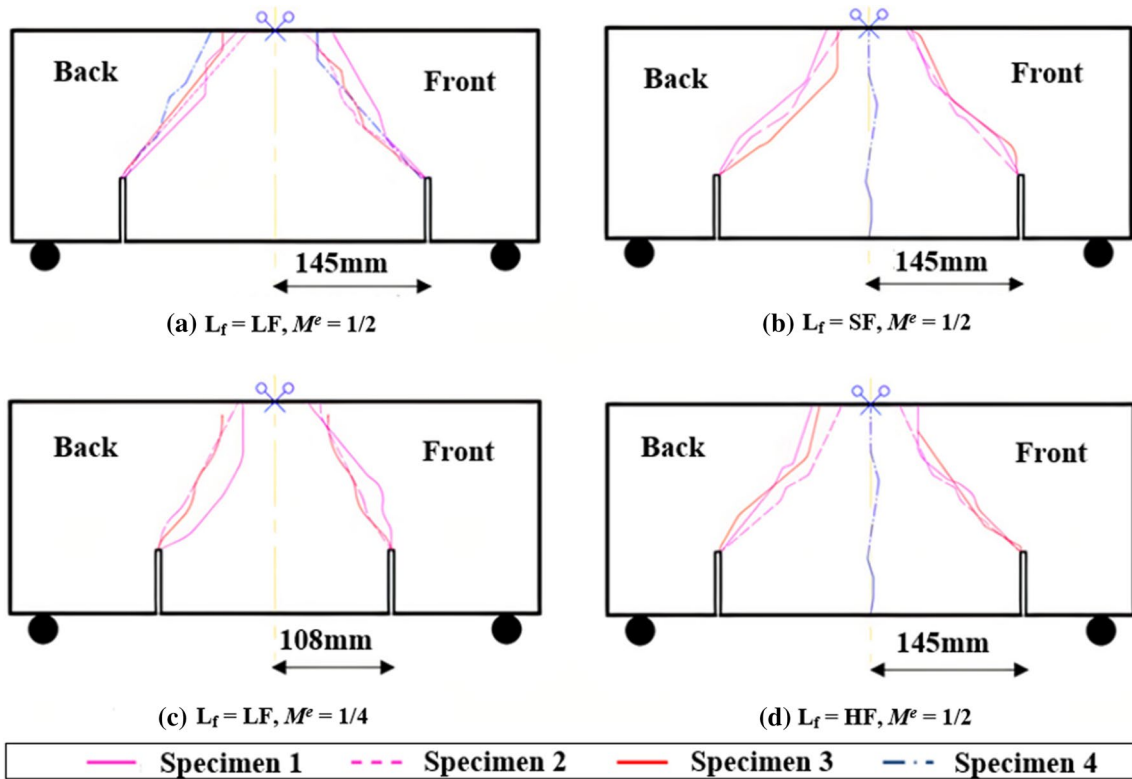
(a) $L_f = LF$, $M^e = 1/2$

(b) $L_f = SF$, $M^e = 1/2$

(c) $L_f = LF$, $M^e = 1/4$

(d) $L_f = HF$, $M^e = 1/2$

— Specimen 1   - - - Specimen 2   — Specimen 3   — · — Specimen 4

Fig. 15 Front and back views of crack trajectories for various fiber lengths and M^e

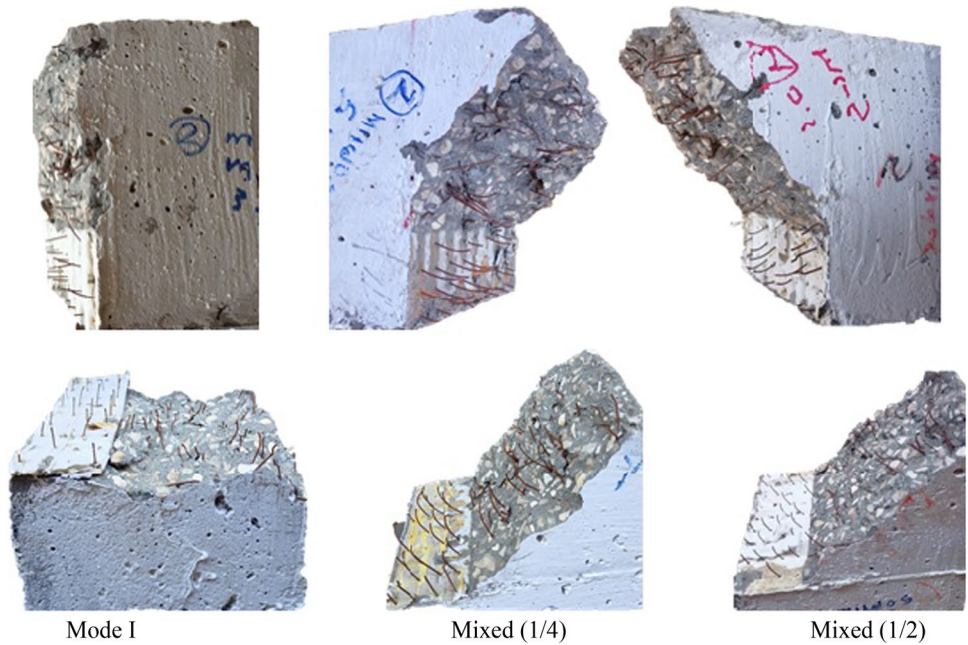**Fig. 16** Fracture surface of MC beams subjected to different modes of mixity

Mode I   Mixed (1/4)   Mixed (1/2)

Table 13 Section analysis of steel fibers number

Beam ID	Mean number of steel fiber[a]	Theoretical number of fibers	Actual percentage %
UN-LF	167 (0.020)	191	43.6
UN-HF	207 (0.090)	236	43.8
UM-SF	229 (0.055)	299	38.3
MC-LF (0)	120 (0.025)	134	44.8
MC-HF (0)	131 (0.047)	165	39.6
MC-SF (0)	142 (0.043)	209	34.0
MC-LF (1/2)	129 (0.052)	162	39.7
MC-HF (1/2)	162 (0.077)	201	40.4
MC-SF (1/2)	179 (0.041)	254	35.3
MC-LF (1/4)	108 (0.081)	148	36.4

[a]Values in the parentheses indicate the coefficient of variance

$$N_S = \alpha_2 * \frac{V_f}{A_{f1}} \tag{3}$$

where N_s is the number of fibers crossing a unit area, A_{f1} is the cross-section area of one fiber, and α_2 is the efficiency orientation factor.

The theoretical number of fibers according to Eq. (3) and the mean number for each specimen are entailed in Table 13. The actual percentage is also calculated and presented in the same table. Based on the section analysis of the present study, the values of α_2 ranged from 0.34 to 0.383 in SF beams, from 0.396 to 0.438 in HF specimens, and from 0.364 to 0.448 in LF beams. The values of α_2 in the present study were around the recommended value by previous studies [55–61]. Lub and Padmoes [55] recommended the value of $(2/\pi)^2$. Gasparini et al. [56], and Stroeven and Hu [57] recommend the value of 0.5. Zandi et al. [58] found that the range of α_2 for the 3D arrangement is between 1/6 to1/2, which includes the values of the present study. Swamy [59] recommended the value of 0.41, which was suggested by Romualdi and Mandel [60]. Gettu et al. [61] studied the orientation and distribution factors using different specimen shapes and compacting methods. Using prisms with the internal vibration method indicated that $\alpha_2 = 0.391$ and 0.428. On the other hand, Wille et al. [62] studied fiber distribution and orientation in ultra-high-performance FRC beams using different fiber lengths. They found that the efficiency factor is greater than 0.59. The increase in their values may be due to using very short fiber and an NMAS of 0.8 mm.

5 Conclusion

The primary goal of this study was to determine the mixed-mode fracture toughness of FRC based on a realistic experimental approach using MC specimens. Based on the analyzed results, the following conclusions can be summarized:

1. The presence of fiber bridging behind the crack tip in MC specimens reflects three different main responses from TTC specimens. Firstly, the crack initiation occurred before the peak load in MC specimens, while it occurred at the peak load in TTC specimens. Secondly, the applied load dropped gradually in MC specimens and sharply in TTC specimens. Thirdly, the ratios of the total energy of the MC specimens to that of TTC specimens subjected to a mixed-mode having $M^e = 0.5$ were 188.6%, 220.5%, and 147% for short, hybrid, and long fibers, respectively. For long fibers and $M^e = 0.25$, this ratio was 217%.

2. The ratios of peak loads between the MC and the TTC specimens subjected to a mixed-mode having $M^e = 0.5$ were 165.63%, 153.95%, and 160.53% for short, hybrid, and long fibers, respectively. For long fibers and $M^e = 0.25$, this ratio was 247.83%. Accordingly, this ratio increased by decreasing M^e, i.e., the efficiency of hooked-end steel fibers to resist mode I crack growth is more pronounced than mode II.

3. For mixed-mode loading, increasing fiber length increased the peak load of MC specimens by about 15.1% as the fiber length increased from 35 to 50 mm. On the other hand, utilization of hybrid fiber increased the peak load by 10.4% compared to short fiber. This may be because the fibers of 50 mm length near the crack mouth suffer from pull-out lower than those of 35 mm length, i.e., they have more efficiency in bridging the crack surfaces.

4. For MC FRC specimens, changing the fracture mode from mode I ($M^e = 0.0$) to mixed mode (I/II) of $M^e = 0.5$ increased K_{eff} by 19.2%, 17.1%, and 18.6% for short, hybrid, and long fibers, respectively. On the other hand, increasing the mode of mixity from 0.25 to 0.5 increased K_{eff} by about 6.1% for long fibers.

5. The ratios of d_{max}/NMAS in the case of MC specimens ranged between one and two.

6. The effect of heterogeneity of FRC on the scattering in crack trajectories was marginal due to the transgranular crack growth of such materials.

7. Based on the section analysis of the present study, the efficiency orientation factor α_2 ranged from 0.34 to 0.383, 0.396 to 0.438, and 0.364 to 0.448 for specimens reinforced with short, hybrid, and long fibers, respectively.

Declarations

Conflict of interest The authors declare that they have no conflict of interest.

Ethical approval This article does not contain any studies with human participants or animals performed by any of the authors.

Informed consent None.

References

1. A.E. Naaman, Fiber reinforced cement and concrete composites, 1st ed., Techno-Press 3000, Sarasota, Florida 34231, USA, 2018.
2. Othman MA, El-Emam HM, Seleem MH, Sallam HE, Moawad M. Flexural behavior of functionally graded concrete beams with different patterns. Arch Civ Mech Eng. 2021;21(4):1–6. https://doi.org/10.1007/s43452-021-00317-0.
3. Knott JF. Fundamentals of fracture mechanics. London: Butterworths & Co publishers Ltd; 1976.
4. Hillerborg A. A model for fracture analysis, Report TVBM 3005. Sweden: University of Lund; 1978.
5. Jenq Y, Shah SP. Two parameter fracture model for concrete. J Eng Mech. 1985;111(10):1227–41. https://doi.org/10.1061/(asce)0733-9399(1985)111:10(1227).
6. Bažant ZP, Oh BH. Crack band theory for fracture of concrete. Matériauxet Constr. 1983;16(3):155–77. https://doi.org/10.1007/bf02486267.
7. Bažant ZP, Kazemi MT. Determination of fracture energy, process zone length and brittleness number from size effect, with application to rock and concrete. Int J Fract. 1990;44(2):111–31. https://doi.org/10.1007/BF00047063.
8. Hillerborg RT. The theoretical basis of a method to determine the fracture energy GF of concrete. Mater Struct. 1985;18(4):291–6.
9. Qian X, Yang W. Initiation of ductile fracture in mixed-mode I and II aluminum alloy specimens. Eng Fract Mech. 2012;93:189–203. https://doi.org/10.1016/j.engfracmech.2012.06.018.
10. Laukkanen, K. Wallin, R. Rintamaa. Evaluation of the effects of mixed mode I-II loading on elastic-plastic ductile fracture of metallic, In: Mixed-mode crack behavior. ASTM special technical publication 1359, Atlanta, USA, 1999. 3–20.
11. Fayed AS, Abd-Alhady AA, Sherbini HS, Sallam HEM. Crack path in steel fiber reinforced concrete composite under mixed mode. ASJCE Fac Eng Ain Shams Univ. 2008;1(1):17–26.
12. Arikan H. Fracture behavior of textile glass fiber reinforced polymer concrete according to mixed-mode. J Thermoplast Compos Mater. 2012;25(6):663–77. https://doi.org/10.1177/0892705711412649.
13. Carpinteri R. Brighenti, Fracture behaviour of plain and fiber-reinforced concrete with different water content under mixed mode loading. Mater Des. 2010;31(4):2032–42. https://doi.org/10.1016/j.matdes.2009.10.021.
14. Zhang HD, Xu XS. Research on test of fracture toughness and fracture criterion of crack of mixed mode I and II of steel fiber concrete. Adv Mater Res. 2013;671:1688–91. https://doi.org/10.4028/www.scientific.net/AMR.671-674.1688.
15. Fett T. Mixed-mode stress intensity factors for three-point bending bars. Int J Fract. 1991;48(4):67–74. https://doi.org/10.1007/bf00012920.
16. He MY, Hutchinson JW. Asymmetric four-point crack specimen. Appl Mech. 2000;67(1):207–9. https://doi.org/10.1115/1.321168.
17. Murakami Y. Stress intensity handbook. Oxford, New York: Pergamon Press; 1987.
18. Zimmermann EA, Launey ME, Barth HD, Ritchie RO. Mixed-mode fracture of human cortical bone. Biomaterials. 2009;30(29):5877–84. https://doi.org/10.1016/j.biomaterials.2009.06.017.
19. Shahani AR, Tabatabaei SA. Computation of mixed mode stress intensity factors in a four-point bend specimen. Appl Math Model. 2008;32(7):1281–8. https://doi.org/10.1016/j.apm.2007.04.001.
20. Jorbat MH, Hosseini M, Mahdikhani M. Effect of polypropylene fibers on the mode I, mode II, and mixed-mode fracture toughness and crack propagation in fiber-reinforced concrete. Theoret Appl Fract Mech. 2020;109:102723. https://doi.org/10.1016/j.tafmec.2020.102723.
21. Razmi MM. Mirsayar, On the mixed mode I/II fracture properties of jute fiber-reinforced concrete. Constr Build Mater. 2017;148:512–20. https://doi.org/10.1016/j.conbuildmat.2017.05.034.
22. Li WH, Peters WFR. Two-phase crack propagation approach to fatigue life prediction of preloaded notched members. Eng Fract Mech. 1986;23(5):793–801. https://doi.org/10.1016/0013-7944(86)90091-3.
23. Li V. CTD criterion applied to mixed mode fatigue crack growth. Fatigue Fract Eng Mater Struct. 1989;12(1):59–65. https://doi.org/10.1111/j.1460-2695.1989.tb00508.x.
24. Hammouda MMI, Sallam HEM. An elastic-plastic finite element simulation of crack tip deformation in fatigue. ICF8, Kiev. In: Advances in Fracture Resistance in Materials, 1996, Int.Congress on Fracture, Vol. 2, Tata McGraw-Hill, New Delhi, India, 3–10. 1993.
25. Hammouda MMI, Ahmad SE, Sallam HEM. Correlation of fatigue crack growth by crack tip deformation behavior. Fatigue Fract Eng Mater Struct. 1995;18(1):93–104. https://doi.org/10.1111/j.1460-2695.1995.tb00144.x.
26. Hammouda MMI, Seleem MH, Sallam HEM, Ahmad SE. Front development of a long fatigue crack during its growth. Fatigue Fract Eng Mater Struct. 1997;20(6):849–62. https://doi.org/10.1111/j.1460-2695.1997.tb01529.x.
27. Hammouda MMI, Ahmad SE, Seleem MH, Sallam HEM. Fatigue crack growth due to two successive single overloads. Fatigue Fract Eng Mater Struct. 1998;21(12):1537–47. https://doi.org/10.1046/j.1460-2695.1998.00117.x.
28. Hammouda MMI, Ahmad SE, Sherbini AS, Sallam HEM. Deformation behaviour at the tip of physically short fatigue crack due to a single overload. Fatigue Fract Eng Mater Struct. 1999;22(2):145–51.
29. Hammouda MMI, Osman HG, Sallam HEM. Mode I notch fatigue crack growth behaviour under constant amplitude loading and due to the application of a single tensile overload. Int J Fatigue. 2004;26(2):183–92. https://doi.org/10.1016/S0142-1123(03)00093-8.
30. Hammouda MMI, Sallam HEM, Osman HG. Significance of crack tip plasticity to early notch fatigue crack growth. Int J Fatigue.

2004;26(2):173–82. https://doi.org/10.1016/S0142-1123(03)00094-X.

31. El-Emam HM, Salim HA, Sallam HE. Composite patch configuration and prestraining effect on crack tip deformation and plastic zone for inclined cracks. J Compos Constr. 2016;20(4):6002. https://doi.org/10.1061/(ASCE)CC.1943-5614.0000655.

32. El-Emam HM, Salim HA, Sallam HE. Composite patch configuration and prestress effect on SIFs for inclined cracks in steel plates. J Struct Eng. 2017;143(5):6229. https://doi.org/10.1061/(ASCE)ST.1943-541X.0001727.

33. Nitschke A. Modeling of load-bearing behavior of fiber-reinforced concrete tunnel linings. Shotcrete Mag. 2017;19(2):28–34.

34. El-Sagheer I, Abd-Elhady AA, Sallam HEM, Naga SA. An assessment of ASTM E1922 for measuring the translaminar fracture toughness of laminated polymer matrix composite materials. Polymers. 2021;13(18):3129. https://doi.org/10.3390/POLYM13183129.

35. ASTM. ASTM E1922-04. Standard Test Method for Translaminar Fracture Toughness of Laminated and Pultruded Polymer Matrix Composite Materials; ASTM: West Conshohocken, PA, USA, 2015.

36. Elakhras AA, Seleem MH, Sallam HEM. Intrinsic fracture toughness of fiber reinforced and functionally graded concretes: an innovative approach. Eng Fract Mech. 2021;258:8098. https://doi.org/10.1016/j.engfracmech.2021.108098.

37. Elakhras AA, Seleem MH, Sallam HEM. Fracture toughness of matrix cracked FRC and FGC beams using equivalent TPFM. Fratturaed Integrità Strutturale. 2022;16(60):73–88. https://doi.org/10.3221/IGF-ESIS.60.06.

38. Elakhras AA, Seleem MH, Sallam HEM. Real fracture toughness of FRC and FGC: size and boundary effects. Arch Civ Mech Eng. 2022;22(2):1–17. https://doi.org/10.1007/s43452-022-00424-6.

39. Ali AYF, El-Emam HM, Seleem MH, Sallam HEM, Moawad M. Effect of crack and fiber lengths on mode I fracture toughness of matrix-cracked FRC beams. Constr Build Mater. 2022;341:127924. https://doi.org/10.1016/j.conbuildmat.2022.127924.

40. Sallam HEM. Crack arresters in steel structure components, M. Sc. Thesis, Zagazig Univ., Egypt, 1990. https://doi.org/10.13140/RG.2.2.14385.43369.

41. Wang H, Wu G, Jiang J. Fatigue behavior of cracked steel plates strengthened with different CFRP systems and configurations. J Compos Constr. 2015. https://doi.org/10.1061/(ASCE)CC.1943-5614.0000647,04015078.

42. ACI Committee 544–3R, Guide for Specifying, Proportioning, and Production of Fiber-reinforced Concrete, American Concrete Institute. 2008.

43. BS EN 12390–3, Testing hardened concrete- Compressive strength of test specimens, Part 3: British Standards. 2019.

44. BS EN 12390–6, Testing hardened concrete. Tensile splitting strength of test specimens, Part 6: British Standards. 2009.

45. Barragan B, Gettu R, Agullo L, Zerbino R. Shear failure of steel fiber-reinforced concrete based on push-off tests. ACI Mater J. 2006;103(4):251.

46. Jongvivatsakul P, Attachaiyawuth A, Pansuk W. A crack-shear slip model of high-strength steel fiber-reinforced concrete based on a push-off test. Constr Build Mater. 2016;126:924–35. https://doi.org/10.1016/j.conbuildmat.2016.09.080.

47. Mubaraki M, Osman SA, Sallam HEM. Effect of RAP content on flexural behavior and fracture toughness of flexible pavement.

Latin Am J Solids Struct. 2019;16(3):1–15. https://doi.org/10.1590/1679-78255516.

48. Chang DI, Chai WK. Flexural fracture and fatigue behavior of steel-fiber-reinforced concrete structures. Nuclear Eng Des. 1995;156(1–2):201–7. https://doi.org/10.1016/0029-5493(94)00946-V.

49. Qing L, Li Y, Wang X, Yu K, Mu R. Investigation of mixed-mode fracture of aligned steel fibre reinforced cementitious composites. Int J Fract. 2021;228(2):159–78. https://doi.org/10.1007/s10704-021-00527-w.

50. Nunes LC, Reis JM. Experimental investigation of mixed-mode-I/II fracture in polymer mortars using digital image correlation method. Latin Am J Solids Struct. 2014;11:330–43. https://doi.org/10.1590/s1679-78252014000200011.

51. Sallam HEM, Mubaraki M, Yusoff NI. Application of the maximum undamaged defect size (d_{max}) concept in fiber-reinforced concrete pavements. Arab J Sci Eng. 2014;39(12):8499–506. https://doi.org/10.1007/s13369-014-1400-4.

52. Abou El-Mal HSS, Sherbini AS, Sallam HEM. Mode II fracture toughness of hybrid FRCs. Int J Concrete Struct Mater. 2015;9(4):475–86. https://doi.org/10.1007/s40069-015-0117-4.

53. Carpinteri A. Stability of fracturing process in RC beams. J Struct Eng. 1984;110(3):544–58. https://doi.org/10.1061/(ASCE)0733-9445(1984)110:3(544).

54. Baluch MH, Azad AK, Ashmawi W. Application of fracture mechanics to reinforced concrete. In Carpinteri A (Ed), CRC Press, p. 24 (1994).

55. Lub KB, Padmoes T. Mechanical behavior of steel fiber-cement mortar in tension and flexure interpreted by means of statistics. Mater J. 1989;86(1):16–28.

56. Gasparini DA, Verma D, Abdallah A. Postcracking tensile strength of fiber reinforced concrete. Mater J. 1989;86(1):10–5. https://doi.org/10.14359/1812.

57. Stroeven P, Hu J. Effectiveness near boundaries of fibre reinforcement in concrete. Mater Struct. 2006;39(10):1001–13. https://doi.org/10.1617/s11527-006-9101-4.

58. Zandi Y, Husem M, Pul S. Effect of distribution and orientation of steel fiber reinforced concrete. In: Proceedings of the 4th WSEAS international conference on Energy and development-environment-biomedicine. pp. 260–264 (2011).

59. Swamy RN. Fibre reinforcement of cement and concrete. Matériauxet Constr. 1975;8(3):235–54. https://doi.org/10.1007/BF02475172.

60. Romualdi JP, Mandel JA. Tensile strength of concrete affected by uniformly distributed and closely spaced short lengths of wire reinforcement. J Proc. 1964;61(6):657–72.

61. Gettu R, Gardner DR, Saldivar H, Barragán BE. Study of the distribution and orientation of fibers in SFRC specimens. Mater Struct. 2005;38(1):31–7. https://doi.org/10.1617/14021.

62. Wille K, Tue NV. Parra-Montesinos, Fiber distribution and orientation in UHP-FRC beams and their effect on backward analysis. Mater Struct. 2014;47(11):1825–38. https://doi.org/10.1617/s11527-013-0153-y.